# Charge gated ion transport through polyelectrolyte intercalated amine reduced graphene oxide membranes

*Xiaoxiao Song* [a]; *Rahul S. Zambare* [b]; *Saren Qi* [c]; *Bhuvana NIL Sowrirajalu* [b]; *Antony Prince James Selvaraj* *[,b]; *Chuyang Y. Tang* *[,d]; *Congjie Gao* [a]

[a] Centre for Membrane and Water Science and Technology, Ocean College, Zhejiang University of Technology, Hangzhou, 310014, China

[b] Environmental and Water Technology Centre of Innovation (EWTCOI), Ngee Ann Polytechnic, 599489, Singapore

[c] Singapore Membrane Technology Center, Nanyang Technological University, 639798, Singapore.

[d] The University of Hong Kong, Department of Civil Engineering, Pokfulam, Hong Kong.

KEYWORDS: Amine reduced graphene oxide; Layer-by-layer; Polyelectrolyte; Charge gated nanochannel; Donnan exclusion.

ABSTRACT

Charge gated channels are nature's solutions for transport of water molecules and ions through aquaporins in biological membranes while excluding undesired substances. The same mechanism has good potentials to be adopted in pressure or electrically driven membrane separation processes. Herein, we report highly charged nanochannels created in polyelectrolyte (PE) intercalated amine reduced graphene oxide membrane (PE@ArGO membrane). The PE@ArGO membrane, with a rejection layer of ~160 nm in thickness, features a laminate structure and a smooth top surface of a low roughness (typically ~17.2 nm). Further, a modified PE@ArGO membrane (mPE@ArGO membrane) was developed in-situ using free chlorine scavenging post-treatment method, which was designed to alter the charge while keeping alteration to the layered structure minimal. The surface charge of the PE@ArGO and mPE@ArGO membrane was +4.37 $mC/m^2$ and −4.28 $mC/m^2$ respectively. In pressure driven processes, the pure water permeability for PE@ArGO and mPE@ArGO was 2.9 L $m^{-2}$ $h^{-1}$ $bar^{-1}$ and 10.8 L $m^{-2}$ $h^{-1}$ $bar^{-1}$ respectively. Salt rejection is highly dependent on the charge density of the membrane surface, the valence of the co-ions and the size of ions in hydrated form. For example, in the positively charged PE@ArGO membranes, the rejection of the salts follows the order of: $R(MgCl_2)$, 93.0% > $R$(NaCl), 88.2% ≈ $R(MgSO_4)$, 88.1% > $R(Na_2SO_4)$, 65.1%; while in the negatively charged mPE@ArGO membranes, the rejection of the salts follows the order of: $R(Na_2SO_4)$, 90.3% > $R$(NaCl), 85.4% > $R(MgSO_4)$, 68.3% > $R(MgCl_2)$, 42.9%. To the best knowledge of the authors, this is the first study to report graphene oxide based membranes (GOBMs) with high density positive/negative charge gated ion transport behavior. What's more, the high rejection rate along with high water permeability of the PE@ArGO and mPE@ArGO membranes has not been achieved by other types of GOBMs.

## 1. Introduction

Membrane technology is one of the most powerful strategies to address the conundrum of water shortage.[1] Nanofiltration, reverse osmosis, and forward osmosis are among the most effective ways to extract clean water from the impaired water.[2] The semipermeable selective layer is the determining factor in the application of membrane separation process, which has been dominated by the conventional polyamide materials over the last few decades.[3] Nonetheless, the relatively rough surface and low water permeability of polyamide based membranes resulted in a high tendency of fouling and high operation costs.[2, 4] In the pursuit of enhanced water permeability and better separation efficiency, researchers have been actively searching for alternative membrane materials which have more ordered structure, less thickness, lower roughness, and tunable pore size.[5]

Graphene oxide (GO) nanosheets have good chemical stability, high water permeability, thin thickness and ion-sieving capability.[6-8] A GO membrane can be assembled by stacking aqueous dispersion of GO nanosheets onto a vacuum filtered paper.[9] The existence of oxygen-containing species (such as hydroxyl, epoxy, and carboxylic groups) creates two-dimensional (2D) channels, whose characteristic interspace is given by the *d*-spacing between GO nanosheets less 0.35 nm (the electron cloud thickness of a graphene nanosheet).[10] The value of the *d*-spacing can vary in the range of 0.8~1.5 nm, according to the hydration status,[11-13] reduction degree,[9, 14-15] and crosslinking degree[12-13, 16-17] of GO nanosheets. The reported NaCl rejection for GO or reduced GO based membranes is typically within the range of 20~40%.[12, 17] Such low rejection has not yet fulfilled the quest for higher performance membranes.[18]

The surface charge of an NF/RO membrane can significantly impact its separation properties.[19-21] Despite the strong evidence that the negative charge of GO impacts salt rejection,[9, 22] the vast

research studies in existing literature have focused on the fine-tuning of *d*-spacing (e.g., in the range of 0.6-0.7 nm for optimized size exclusion of salts.[6, 12-13, 15, 23] ). Few attempts have been made to design desirable charge property and density in the GOBMs. In a recent work, GO nanosheets were assembled directly by polyallyamine (PAH) molecules using multiple layer-by-layer method (mLBL),[24] which provides a potential way to investigate the effect of charge repulsion in GOBMs. Unfortunately, due to the strong positive charge of PAH molecules, GO nanosheets tend to be folded into micro-sphere like structures; the lack of well-structured GO channels complicates the interpretation of the role of charge on membrane separation performance. Moreover, the reported assembly process relies on concentrated GO/PAH (1000 mg/L) solutions and numerous cycles. Up to day, it remains a critical challenge to prepare stable GOBMs with ordered multi-layer structure, well-defined water channels, and good long-term stability for water filtration.[25-27]

To overcome these challenges, we designed positively charged PAH@ArGO nanosheets, which can be readily dispersed in aqueous solutions, and assembled them into PE@ArGO membranes low roughness. We hypothesize **t**hat the enhanced charge density introduced by intercalated polyelectrolyte, and their charge properties would have a major impact on the ion rejection of PE@ArGO membranes. Furthermore, we applied *in-situ* chlorine oxidation to introduce negative charge without significantly altering the layered structure. Overall, our study provides novel insights in the facile fabrication of GOBMs with tunable intercalated charges, continuously ordered and multi-layered structure, and long-term stability in water. The contrast between the positively charged and negatively charged GOBMs further enable us to better understand the combined effects of size exclusion and charge repulsion on their salt rejection performance.

## 2. Materials and methods

2.1 Synthesis of GO, ArGO, PAH@ArGO, and PSS@GO nanosheets. Chemicals were purchased from Sigma-Aldrich Singapore unless specified otherwise. The GO was synthesized by a modified Hummer's method according to our previous publication.[28] A typical synthesis route is described in Supporting information (SI, Page S2). Next, The positive charge on PE@ArGO was introduced through a two-step strategy: First, GO nanosheets were reduced and grafted with ethylenediamine (EDA) moieties, forming amine reduced graphene (ArGO); Afterwards, the charge density was further enhanced by anchoring poly (allylamine hydrochloride) (PAH) molecules on the ArGO (PE@ArGO).

The Haddon's method was adopted to graft ethylenediamine (EDA) on a reduced GO nanosheets with a high conversion rate of -COOH to –CONH-.[29]

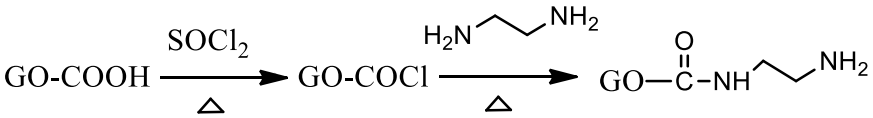


First, freeze-dried GO powder (50 mg) was dispersed in N, N-Dimethylformamide (DMF) (Anhydrous, 99.8%) with in an ultrasound bath (Elmasonic E60H) for 3 hours. Then, 5 ml $SOCl_2$ (ReagentPlus, ≥99%) was added to the GO/DMF dispersion, and the mixture was refluxed at 70 °C for 12 h. Afterwards, the acylated GO (GO-COCl) was separated from unreacted $SOCl_2$ with a 0.45 μm PTFE filter (Merck Millipore), washed with DMF repeatedly, and re-dispersed in 60 ml DMF. EDA (ReagentPlus, ≥99%) was added dropwise into the GO-COCl/DMF mixture, and the amidation reaction was continued with stirring at 80 °C overnight. The ArGO product was filtered, washed with ethanol and DI water several times, and purified by centrifuging at 8000 rpm to remove any insoluble sediments. Finally, the ArGO in the supernatant was collected and redispersed. PAH@ArGO dispersion was formed by dissolving PAH (average $M_w \sim 50$ kDa) in

the ArGO dispersion by stirring at 25 °C for at least 30 min. The weight ratio of PAH:ArGO was kept at 10:1. Similarly, PSS@GO dispersion was prepared by dissolving PSS ($M_w$ ~ 70 kDa) into GO dispersion.

2.2 Fabrication of ArGO, PE@ArGO, and mPE@ArGO membranes.

ArGO and PE@ArGO membranes were formed on top of the commercial track etched polycarbonate membranes (Millipore PCTE, 100 nm) using a vacuum filter holder (Advantec, 47mm). As the assembly procedure is similar for PE@ArGO and ArGO membranes, only the formation of PE@ArGO membrane is discribed below and the fabracation details for ArGO membrane can be found in SI (Page S2). The PE@ArGO membrane is fabriated by the polyelectrolyte assisted vacuum filtration (PE-VF) process in a layer-by-layer (LbL) manner (Scheme 1). Prior to the PE-VF process, concentrate NaCl solution was added gradually to the PE@ArGO dispersion to increase ionic strength. This method was adopted from our previous work to increase the effectiveness of PE deposition.[30] In the PE-VF (+) solution, the final composition is NaCl (0.5 M), PAH (100 mg/l), and ArGO (10 mg/l). In the PE-VF (−) solution, the final composition is NaCl (0.5 M), PSS (100 mg/l), and GO (10 mg/l). First, 30 ml of PE-VF (+) solution was coated on the substrate membrane, forming PE@$ArGO_{0.5}$. Afterwards, a bilayer of 30 ml of PE-VF (−) and 30 ml PE-VF (+) was coated further to form PE@ArGO. Hence, a complete PE@ArGO membrane contains two layers of PAH@ArGO and one intermediate layer of PSS@GO, which acts as an electrostatic crosslinking layer and enables more deposition of PAH@ArGO in the subsequent layer.

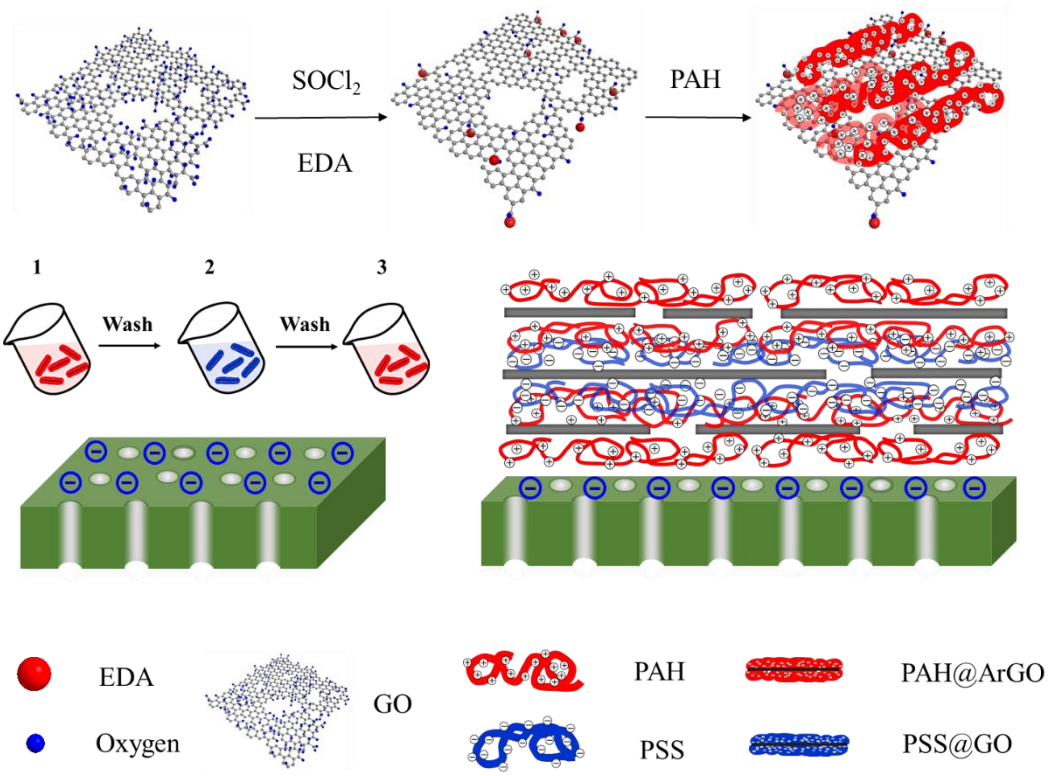


**Scheme 1.** A schematic illustration of the synthesis route for PE@ArGO membrane.

An in-situ free chlorine post treatment method was selected to switch the positive charge of the PE@ArGO membrane to negative charge. Briefly, the PE@ArGO membrane coupon was soaked in 1000 ppm sodium hypochlorite (NaOCl) aqueous solution for 15 min, washed thoroughly and stored in DI water. The resultant hypochlorite-modified membrane is termed as the mPE@ArGO membrane.

2.3 Characterizations. TEM images for dispersed ArGO and PAH@ArGO nanosheets were obtained using JEOL TEM 2100 equipment. Aqueous ArGO samples are drop-casted on a copper grid and then dried in the desiccator for 24 hours before analysis. AFM images for dispersed GO/ArGO/PE@ArGO nanosheets are taken on a Bruker unit (ICON, Peak-force Mode) with freshly cleaved mica as substrate. The surface roughness of membranes was determined by AFM (Park XE-100, Non-contact mode). The roughness data of the membrane are measured based on

membrane area of 25 $\mu m^2$. Non-contact cantilever (PPP-NCHR 10 M) was used with a resonant frequency of 330 kHz and a force constant of 42 N/m. XPS spectrum was analyzed by a Thermo Escalab 250Xi unit with an X-ray source of Al Ka (1486.6 eV), element ratio of C, N, O element is calculated by dividing peak area of C1s, N1s and O1s with their sum. For membrane samples, the surface was etched by an ion beam for 20 seconds before sampling. FTIR for all samples was characterized by a Shimadzu FTIR-8400S. Dispersed nanosheets are drop cast on a silicon chip, dried, and observed in an ultrahigh-resolution Hitachi 8010U FESEM unit in the decelerating mode. FESEM analysis for membrane surfaces and cross sections were obtained using a JOEL FESEM 7600F unit. Cross-section samples were prepared by fracturing the membrane samples in liquid $N_2$ and coated slightly for 30 seconds to minimize the interference of Pt nanoparticles to observation. pH dependent Zeta potential of ArGO/GO suspension (0.2 mg/ml) was determined using a Zetasizer NanoZS (Malvern Instruments Limited, UK). Particle size and surface zeta potential of GO, ArGO, PSS@GO, and PAH@ArGO are analyzed using a Brookhaven Omni unit using the DLS and PALS module respectively. Zeta potential, $\zeta$, for all membrane surfaces was determined by Anton Paar Surpass using an adjustable gap cell (20 mm × 10 mm).[30] For all tests, the electrolyte solution was 1 mM NaCl.

The charge density ($\delta_s$) of the PE@ArGO membranes was derived from the value of kinetic zeta potential, $\zeta$, using the Gouy Chapman equation[31]:

$$\delta_s = \frac{2\varepsilon\lambda \mathrm{kT}}{ze}\sinh\left(\frac{ze\xi}{2kT}\right)$$

Where $\varepsilon$, $\lambda$, $k$, $T$, $z$, $e$ is dielectric constant, debye length, boltzmann constant, absolute temperature, charge number, and the electron charge, respectively.

2.4 Salt and dye rejection test for ArGO, PE@ArGO, and mPE@ArGO membranes. The salt rejection test was performed using a standard commercial stirred cell (Amicon cell 8010) with an effective evaluation area of 3.8 $cm^2$. The stirred cell is connected to an upstream storage tank which supplies feed solution continuously. An $N_2$ gas cylinder was used to provide a pressure between 0 – 6 bar from inlet of a 500 ml storage tank. The cell was stirred at 300 rpm during all tests to alleviate the external concentration polarization (ECP). The feed solution concentration of $MgCl_2$, $MgSO_4$, NaCl and $Na_2SO_4$ solution was constantly at 1mM. The water flux, $J_w$ and the salt rejection ($R$) were calculated using following equations: $J_w=V/(A\times t)$, and $R=1-C_p/C_f$, where $V$ is the total volume of permeate ($L$), $A$ is the effective membrane area ($m^2$), t is the filtration period (h), $C_p$ and $C_f$ is the concentration of permeate and feed solution (g $L^{-1}$) respectively.[32] Salt concentrations were determined by a conductivity meter (S230, Mettler-Toledo, Singapore). The feed solution concentration for Methylene Blue (MB), Rhodamine B (RB), Congo Red (CR), Reactive Black 5 (RB5), and Direct Red 80 (DR80) was constantly at 10 ppm. Continuous dye rejection performance test was conducted with 500 ml of feed solution (RhB for cationic dye and DR 80 for anionic dye) using mPE@ArGO membrane until 250 ml of filtrate was collected. At the filtration volume ($V_f$) of 50, 100, 150, 200, and 250 ml, both retentate and filtrate solutions are collected and analyzed with UV-Vis spectroscopy. The concentrations of dye solutions were determined using a double-beam UV−vis spectrometer (UV-1800, Shimadzu).[33] For all tests, data were repeated for three times, and the average value is reported. The pure water permeability (PWP) of the membrane can be determined based on the Hagen-Poiseuille model: $J_w=(r_P^2/8\mu)\times(A_k/\Delta x)\times\Delta P$, where $J_w$ is the transmembrane water flux (L $m^{-2}$ $h^{-1}$), $r_P$ is the pore radius, $\mu$ is the dynamic viscosity of water at 25 ºC ($8.9*10^{-4}$ Pa*S); $A_k$ is the nominal porosity of the membrane surface; $\Delta x$ is the effective thickness of the membrane; $\Delta P$ is the applied pressure less

the osmotic pressure in the filtration cell. In this equation, PWP (L $m^{-2}$ $h^{-1}$ $bar^{-1}$) equals the product of $r_P^2/8\mu$ and $A_k/\Delta x$.[32] The interfacial free energy ($-\Delta G_{SL}$, mJ $m^{-2}$) was determined based on Young-Dupre equation: $-\Delta G_{SL}=\gamma_L\times(1+SAD+\cos\theta)/(1+SAD)$, where θ is the contact angle, SAD is the surface area difference, and $\gamma_L$ is the pure water surface tension (72.8 mJ $m^{-2}$ at 25°C).[34] For $0°\leq\theta\leq90°$, the larger value of $-\Delta G_{SL}$ suggests a more hydrophilic surface.[35]

2.5 Donnan exclusion theory. Donnan exclusion theory can effectively explain the ions transport through charged membrane.[36] This model emphasizes the contribution of the surface charge to the exclusion of ions but neglect the steric effects. Consider a model salt AB, where $Z_A$ and $Z_B$ is the cation valence number and the anion valence number respectively. The Donan exclusion theory for a negatively charged membrane can be expressed as:

$$R=1-\frac{C_B^m}{C_B}=1-\left(\frac{|Z_B|C_B}{|Z_B|C_B^m+C_X^m}\right)^{|Z_B|/|Z_A|}$$

Wherein, $Z_A$, $Z_B$ is the valence for counterion and co-ion respectively. $C_B$ and $C_B^m$ is the co-ion centration in bulk and in the membrane phase respectively. $C_X^m$ is the fixed charge concentration on membrane surface. Similarly, for positively charged membrane, we have:

$$R=1-\frac{C_A^m}{C_A}=1-\left(\frac{|Z_A|C_A}{|Z_A|C_A^m+C_X^m}\right)^{|Z_A|/|Z_B|}$$

For salt formed by multivalent ions, its form can be expressed as $AB_n$ (where $|Z_A/Z_B|=Z^+/Z^-=n$) or $A_nB$ (where $|Z_B/Z_A|=Z^-/Z^+=n$). When other membrane properties are kept unchanged but only reverse the charge on the membrane, the rejection of $AB_n$ for positively charged membranes should be the same with that of $A_nB$ for negatively charged membrane due to the symmetry of the above two equations.

## 3. Results and discussion

3.1 Characterization of GO, PSS@GO, ArGO, and PAH@ArGO nanosheets. The as-synthesized GO dispersion in water exhibited bright golden color. The C1s XPS spectrum of the GO shows C−O peak (286.6 eV, hydroxyl/epoxy groups) and C=O peak (288 eV, carbonyl groups) with a ratio of 3.0 (Figure 1a). Oxygen accounts for ~31.4% element content in the GO powder, suggesting a high degree of oxidation. The FTIR spectrum (Figure 1d) of the GO powder shows typical characteristic peaks for C=C vibration (~1624 $cm^{-1}$), C=O vibration (~1727 $cm^{-1}$), and O-H vibration (~3397 $cm^{-1}$). The wide broad absorption band at 1000−1500 $cm^{-1}$ are contributed by C−O−C (~1075 $cm^{-1}$), phenolic C-O (~1240 $cm^{-1}$) and C-OH (~1400 $cm^{-1}$).[10] In aqueous solution, GO particles show a strong negative zeta potential in a wide pH range (2.5−10) due to the dissociation of $H^+$ from −COOH and phenolic −OH.[22]

During acylation of GO flakes, the color of the GO dispersion changed from goldish yellow to dark brown. Then, heating with slow addition of EDA turned the color into black (Figure 1b, insert). In XPS spectrum, O/C ratio decreased significantly from 0.46 to 0.07, while N/O ratio increased from ~ 0 to ~ 0.9 (Table 1). The C-O peak weakened substantially (Figure 1b), possibly resulting from the significant reduction of the C−O−C bond at alkali conditions.[37] For ArGO, distinctive new absorption peaks for C−N (950 to 1250 $cm^{-1}$), N−H (1575 $cm^{-1}$), C−H (near 2900 $cm^{-1}$) and N−H (near 3300 $cm^{-1}$) are observed in FTIR spectrum (Figure 1d). Meanwhile, the FTIR peaks for oxygen-containing moieties are no longer observed. Evidence from XPS and FTIR suggest that the GO is successfully bonded with EDA molecules. Due to the protonation of covalently linked $–NH_2$ groups,[38] the ArGO nanosheets have an IEP at pH ~ 9.5 (Figure S1), which falls in the typical $pK_a$ range polyamines.[39] XPS spectrum for the PSS@GO and PAH@ArGO dry powder shows clear characteristic peaks of S 2p and Cl 2p, respectively (Figure 1c). In FTIR spectra, new

peaks occurred for PSS@GO at 1035 $cm^{-1}$ and 1006 $cm^{-1}$ are assigned to characteristic stretching vibration of the $-SO_3^-$ group in PSS; and new peaks occurred for PAH@GO at 2910 $cm^{-1}$ and 3373 $cm^{-1}$ are assigned to characteristic stretching vibration of $-CH_2-$ and $-NH_2$ in PAH molecules (Figure 1d).[40]

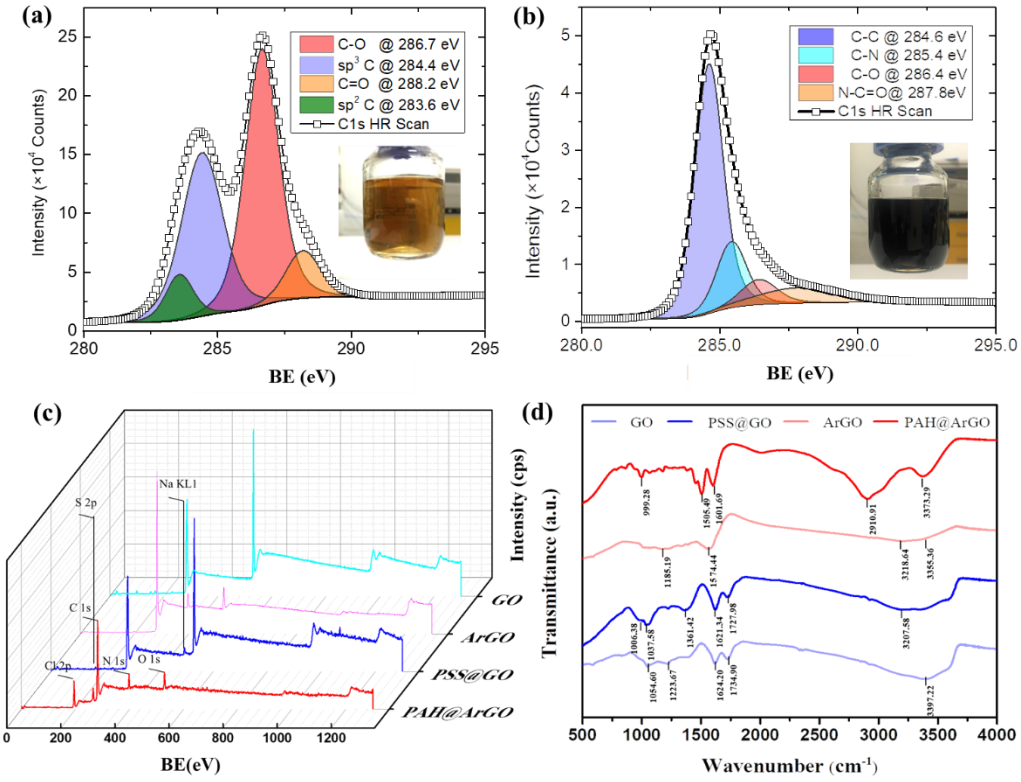


**Figure 1.** XPS high-resolution C1s scan for (a) GO and (b) ArGO powder (insert photo shows the aqueous dispersion of GO and ArGO, respectively); (c) XPS wide spectrum scan of GO (cyan), ArGO (magenta), PSS@GO (blue), and PAH@ArGO (red) powder; (d) FTIR spectrum of GO, ArGO, PSS@GO, and PAH@ArGO powder.

The GO, PSS@GO, ArGO and PAH@ArGO nanosheets can be dispersed well in aqueous solution at a concentration of 1 mg/ml. Figure 2 shows the FESEM image of the nanosheets drop casted on a silicon chip. The dispersion patterns for GO, PSS@GO, and the ArGO are similar,

with nanosheets (mostly 0.5 microns to 3 microns) scattered on surface. In contrast, the PAH@ArGO nanosheets have a tendency to stack up into a few layers and form “islands” of nanosheets. DLS and PALS measurements were taken to analyze the bulk size distribution and surface zeta potential of these nanosheets. As shown in Figure 2e, the effetive size of nanosheets in GO suspension is 369 nm while that for PSS@GO is 433 nm. Although the effective size does not represent the actual physical dimension of 2D materials such as GO nanosheets, the shift of the average size indicate that the light scattering of nanosheets shift to larger effective diameter due to the anchoring of PSS molecules on GO nanosheets. Simlarly, the effective size of PAH@ArGO is 609 nm, much larger than that of ArGO (262 nm). The effective size difference between PAH@ArGO and ArGO is significantly larger than that between PSS@GO and GO, this could be explained by the stacking behavior of PAH@ArGO sheets as observed in Figure 2d. At experimental pH, the ArGO and GO dispersion has a zeta potential of -39.2 mV and 37.5 mV respectively, after anchoring of polyelectrolytes, the value was enhanced to -84.4 mV and 105.4 mV respectively.

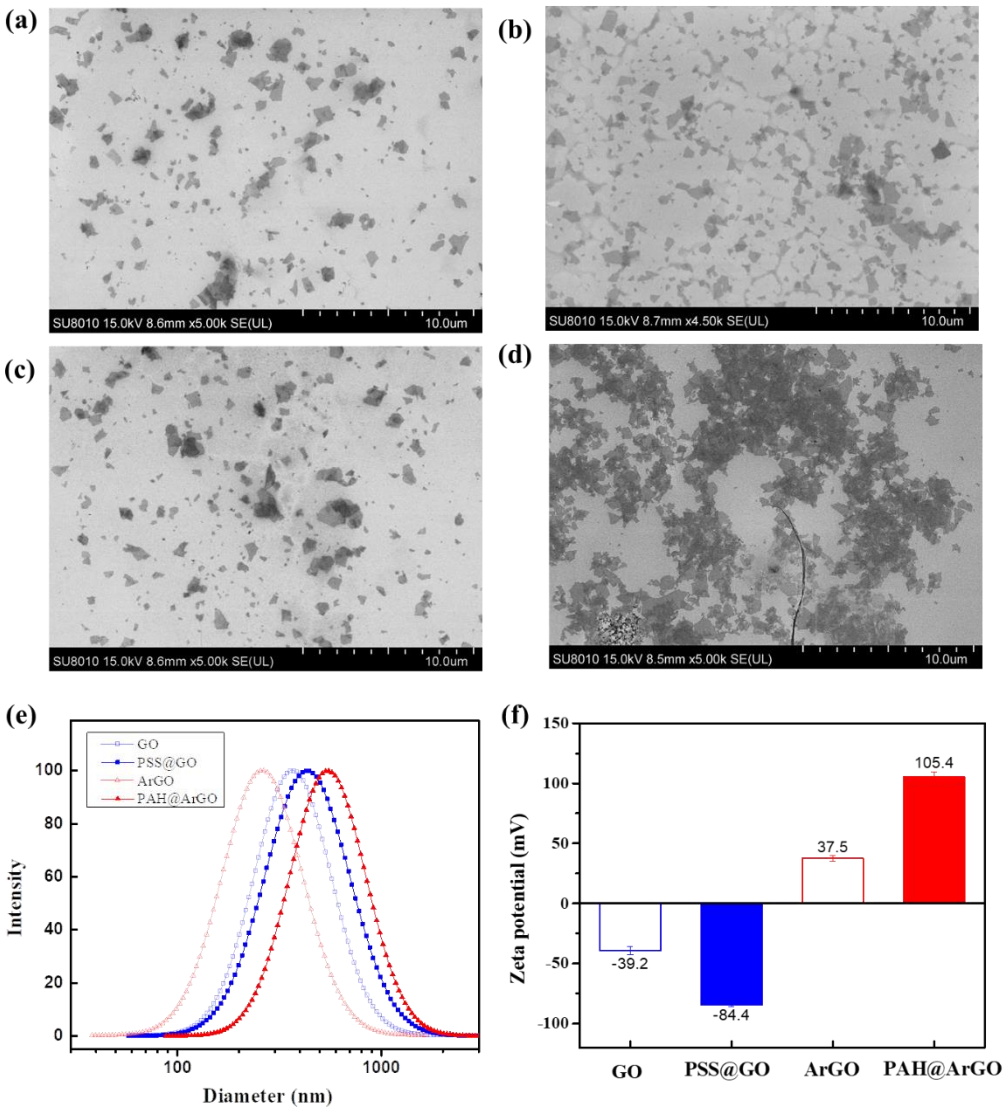


**Figure 2.** The FESEM images of the (a) GO, (b) PSS@GO, (c) ArGO, and (d) PAH@ArGO. Samples were prepared by spreading a drop of suspension on a silicon chip. (e) the lognormal size distribution measured in DLS module; (f) the surface zeta potential measured in PALS module.

A single GO nanosheet has a smooth surface and a thickness of ~ 1 nm, as indicated by the inserted line profile (Figure 3). The root mean square (RMS) of the GO nanosheet is 0.12 nm with 0.02% surface area difference (SAD). PSS@GO nanosheet resembles the morphology of the GO nanosheet, but its thickness is higher (~1.72 nm). By contrast, the ArGO nanosheet shows sinuous

morphology, indicating the inhomogeneity introduced during acylation and amidation. These nanostructures result in an RMS of 0.44 nm and a SAD of 2.19%. Due to the modification, its thickness has been increased to ~2.64 nm. For PAH@ArGO nanosheet, the overall thickness increased further to 4.42 nm (Figure 3). The RMS for the PAH@ArGO nanosheet is 0.94 nm with a SAD of 1.87%. The PAH@ArGO is characterized by a rugged grass-like nanostructure, which resembles the morphology of a PAH/GO composite in a previous study.[41] This suggests the PAH molecules are successfully anchored on ArGO nanosheets and modified the surface. Considering the stacking up behavior of PAH@ArGO nanosheets, it is thus inferred that although ArGO surface is overall positively charged, the localized negative charge carried by unreacted oxygen-containing groups can still interact with strongly positively charged PAH molecules.

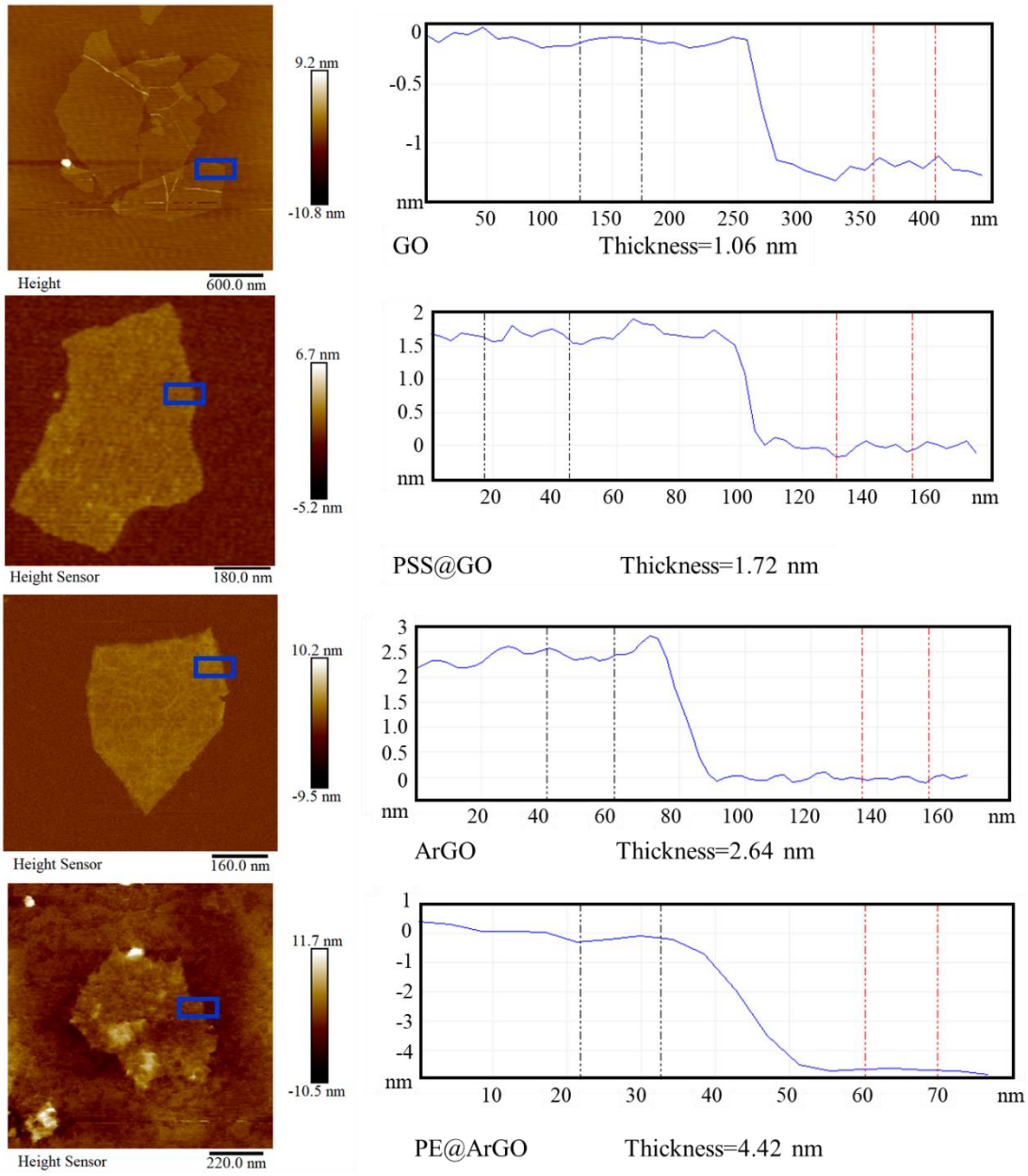


**Figure 3.** The thickness of GO, PSS@GO, ArGO, and PAH@ArGO nanosheets indicated by AFM depth profiles. The blue square indicate the approximately location of the line profile.

3.2 Characterization of ArGO, PE@ArGO, and mPE@ArGO membranes. ArGO nanosheets tend to repel each other in aqueous dispersion because of the positive charge. The ArGO nanosheets are observed to loosely stack on each other (Figure 4). As the RMS of ArGO is significantly higher than the GO, it is presumably much harder to form an as densely stacked

membrane as GO due to much weaker π-π interaction and hydrogen bonding. Hence, negatively charged GO was used as an adhesion and stabilization layer for ArGO through the LbL assembly process due to the interaction between positively and negatively charged groups.[42-43] FESEM image of $ArGO_{0.5}$ membrane surface shows that the pores on the substrate are completely blocked due to the much larger lateral dimension of ArGO nanosheets (Figure S2). The edges of ArGO nanosheets are observed; this indicates the ArGO nanosheets are only weakly bonded to the surface rather than having strong interactions with each other. Such loosely stacked structure could lead to the possible formation of micro-defects on the edge of ArGO nanosheets.[44] As a comparison to $ArGO_{0.5}$ membrane, the ArGO membrane surface finds fewer edges of ArGO nanosheets and is characterized by a wave-like structure similar to the GO membranes. Hence, it is reasoned that the addition of the GO adhesion layer helped to smoothen the surface morphology and bind ArGO nanosheets together.

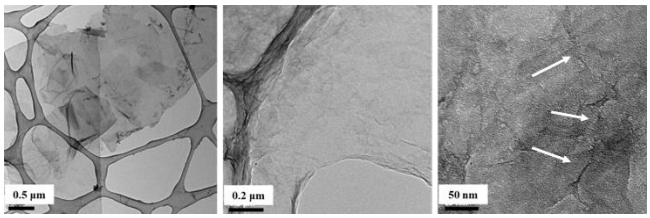


**Figure 4.** The TEM image of ArGO, PE@ArGO, and PE@ArGO (at higher magnification). The white arrow indicates the junction area of adjacent ArGO nanosheets.

Compared with purely ArGO, PE@ArGO nanosheets tend to form an integral thin film, as shown by the PE@ArGO nanosheets coated on a TEM grid (Figure 4). At higher magnification TEM image, the edges of the ArGO nanosheets appear to be "stitched" together (indicated by white arrows). As AFM confirms the modification of ArGO nanosheets by PAH molecules, they should bridge two stacked ArGO nanosheets due to electrostatic interactions between protonated $-NH_2$ and the residue carbonyl/hydroxyl groups on the ArGO nanosheets.[45-46] As a result, the

PE@ArGO$_{0.5}$ membrane surface features a rather smooth and uniform morphology (Figure S2). After the deposition of the subsequent layers, the PE@ArGO membrane showed a slightly rougher surface featuring nano-sized particles (Figure 5a), which is typically formed by strongly charged PAH/PSS pair.[30] Overall, the PE@ArGO membranes are much more tightly-assembled and smoother than the ArGO membranes. No wrinkles and bubble-like structures are observed, although they regularly form on conventional loosely stacked GO based membrane surfaces.[47] This is likely due to that the high charge density of PAH molecules favors the disperse and stretch of the ArGO nanosheets.[22]

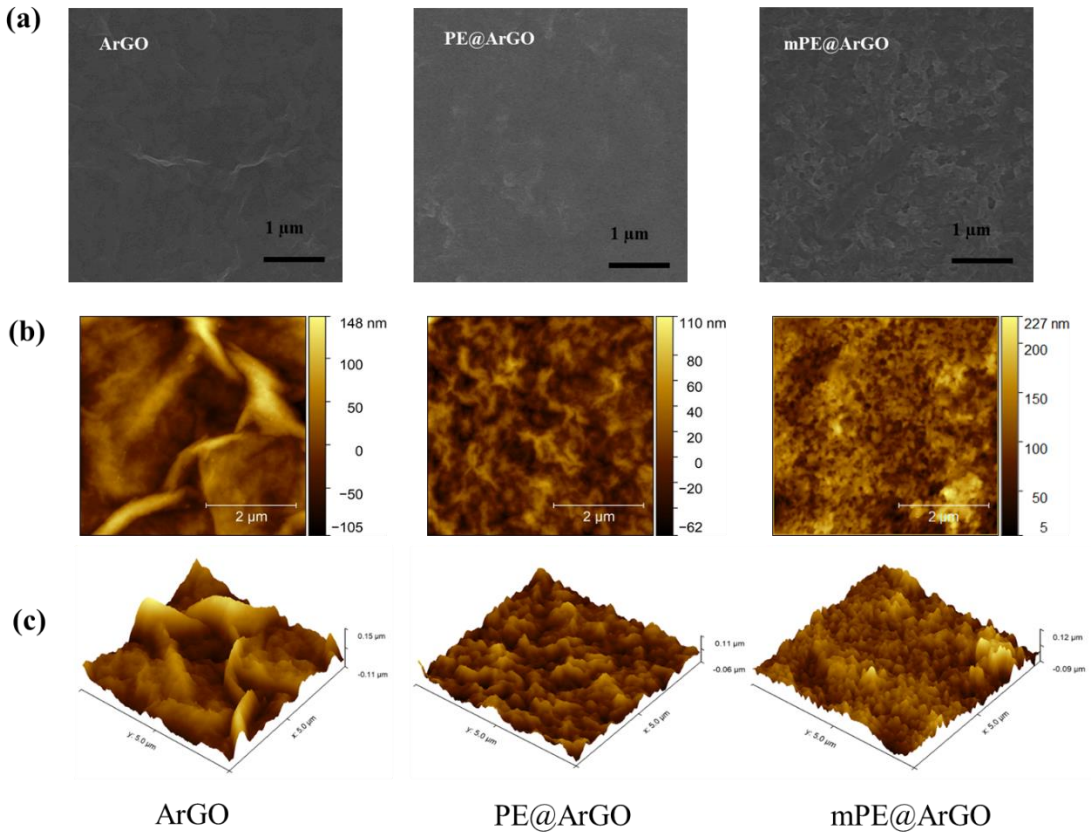


**Figure 5.** (a) The FESEM image; (b) AFM image; and (c) 3D representation of ArGO, PE@ArGO, and mPE@ArGO membrane surface.

The PE@ArGO membrane appears uniform and semi-transparent (Figure 6e). The contact angle of the membrane surface is 42.3° (Figure S3). As probed by AFM, the RMS roughness, $R_q$, is 19.2 nm (Table 2, Figure 5c). The low roughness surface of PE@ArGO membrane is comparable with the commercial NF membranes[48-49] and much lower than the reverse osmosis membranes.[32] Such low roughness is beneficial to fouling-resistance and prolong the lifetime of the membrane.[4] The rejection layer of the PE@ArGO membrane, with a thickness of approximately 160 nm, is bonded with the PCTE substrate membrane (Figure 6a). The well-defined multi-layered structure of the PE@ArGO membrane can be visualized in a decelerating mode FESEM image (Figure 6b), which directly proves that ArGO nanosheets are orderly and densely stacked up during PE assisted assembly rather than aggregating loosely in a random form. Such ordered frameworks are in favor of forming water channels in between ArGO nanosheets. In addition, the dense layered structure maximizes the contact between ArGO nanosheets so that PAH can efficiently bond the nanosheets together through inter-molecular forces. Furthermore, as the oxygen-containing groups of ArGO are significantly reduced, the delamination due to hydration of conventional GO membranes in aqueous environment is minimized. The performance of PE@ArGO was stable after 3 months soaking in water.

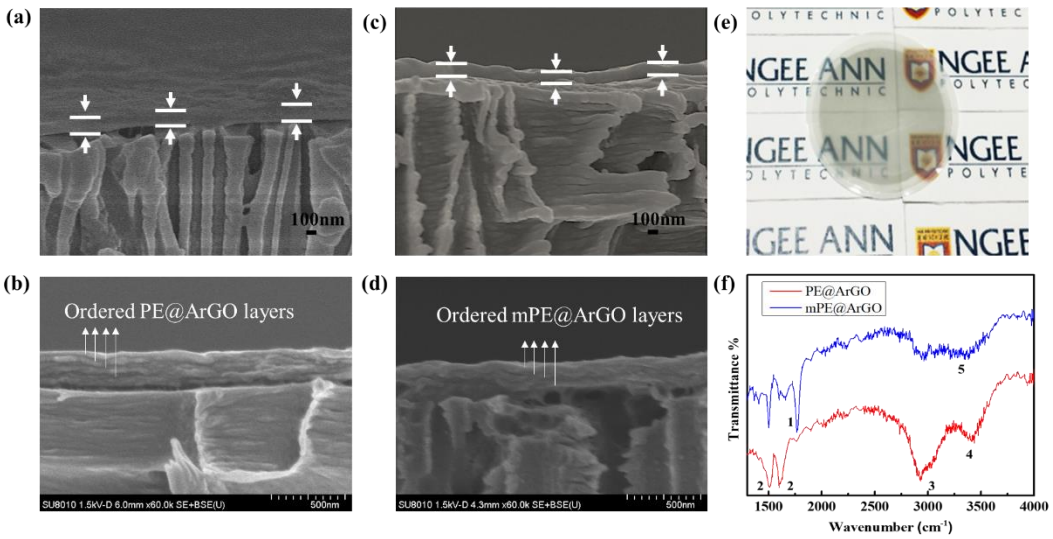


**Figure 6.** PE@ArGO membrane cross section FESEM image observed in (a) normal mode and (b) decelerating mode; mPE@ArGO membrane cross section FESEM image observed in (c) normal mode and (d) decelerating mode; (e) A photo of the semi-transparent PE@ArGO membrane; (f) FTIR spectra and main peaks assignment of the PE@ArGO and mPE@ArGO membranes (see Table 3);

The mPE@ArGO membrane was formed by treating the PE@ArGO membrane with NaOCl. After chlorine modification, the $R_q$ increased slightly to 24.3 nm (Figure 5c), which is mainly contributed by the "scale-like" microstructures (Figure 5a). At the same time, the thickness of the ArGO layer was reduced to approximately 120 nm (Figure 6c). After the treatment, the dense, layered structure of mPE@ArGO membrane maintained (Figure 6d), which is essential for the formation of ordered, negative charge gated ion channels. XPS analysis results (Table 1) suggest that the oxygen content of the mPE@ArGO membrane surface (4.9%) doubled compared with the PE@ArGO membrane (2.4%). The contact angle decreased from 42.3° to 35.8°. These results can be explained by the N−chlorination which results in a more negatively charged, and more hydrophilic membrane surface.[50-53] The more negative charged surface can possibly involve the

inability of protonation for N−Cl,[54] the absorption of $Cl^-$ and $OH^-$ to the membrane surface,[55] and the degradation of primary amine groups into a series of possible oxygen-containing species after being oxidized by NaOCl, such as aldehyde, carboxyl, nitro, and nitroso groups.[56-57] In accordance, FTIR results show the C=O stretching absorption peaks (~1750 $cm^{-1}$) and weakened $-NH_2$ bending peaks near 1520 $cm^{-1}$ and 1625 $cm^{-1}$ (see Figure 6f and Table 3). As penetration of IR is in the micron range, the modification should have had effect on the entire depth of mPE@ArGO membrane, similar with the findings in previous publications that chlorine modifies the entire polyamide layer effectively.[50-52, 58]

3.3 Membrane surface charge. Membrane surface zeta potential is dependent on the pH value. For example, the PE@ArGO membrane is highly positively charged at low pH value because of protonation of $–NH_2$ groups,[42] until the IEP point of pH~9.5 is reached (Figure 7a). The membranes are further tested in DI water environment (pH~5.6), hence the reported ζ values of membranes hereafter are at pH=5.6 unless specified otherwise. The as-assembled ArGO membranes only carry weak surface charge (ζ = +3.4 mV for $ArGO_{0.5}$ and ζ = +11.2 mV for ArGO), although the dispersed ArGO nanosheets are more positively charged (ζ = +39 mV, pH=5.6) (Figure S1). This is because the carboxylic functional group occupies only a small fraction (e.g., the ratio of C=O and C-O absorption peak area intensity is about 1:3, Figure 1a). Hence, the limited availability of carboxylic sites to bind with EDA molecules results in a relatively low charge density. As a result, the negative charged PCTE substrate (ζ = −17 mV) is poorly shielded. After coating with PAH molecules, however, the PE@ArGO membrane surface carries a much higher positive charge of +51.4 mV. Interestingly, the positively charged surface was switched to be strongly negative after NaOCl treatment (mPE@ArGO membrane, ζ = −50.6 mV). According to the Gouy-Chapman equation, the charge density, $\delta_s$, on the PE@ArGO and mPE@ArGO

membrane surface was determined to be +4.37 mC/m$^2$ and −4.28 mC/m$^2$ respectively. As a comparison, the ArGO membrane surface carries only a charge of +0.82 mC/m$^2$. Note that the absolute $\delta_s$ values on PE@ArGO and mPE@ArGO membranes are similar, while the absolute $\delta_s$ value on ArGO membrane is significantly lower. These results suggest that the highly dense charge groups on polyelectrolyte have efficiently modified the ArGO surface, resulting in a fivefold increase of $\delta_s$.

3.4 PWP of the PE@ArGO membranes. The $J_w$ is ploted as a function $\Delta P$ (Figure 7b). The PWP (slope for the $J_w$−$\Delta P$ curve) for the PCTE substrate was 334.8 L m$^{-2}$ h$^{-1}$ bar$^{-1}$. After deposition of PE@ArGO and mPE@ArGO coatings, the PWP value was 2.9 and 10.8 L m$^{-2}$ h$^{-1}$ bar$^{-1}$ respectively, which lies in the typical nanofiltration membrane range. The water permeability of both PE@ArGO and mPE@ArGO membranes is higher than the LbL assembled PAH/PSS membranes in our previous study although the deposited cycles are significantly less.[30] Although the mPE@ArGO carries an opposite charge, the WCA and roughness are not significantly different with that of PE@ArGO membranes, leading to a similar surface free energy (Table 2). Hence, the higher water flux of mPE@ArGO should result from its larger pore radius, according to the Hagen-Poiseuille equation (See section 2.4). In this case, the increase of pore size could be explained by the weakened polyelectrolyte-water hydrogen bonding[59-60] and possible breakage of the chains due to N-chlorination and oxidation.[57, 61] These changes weakened the ability of polyelectrolyte molecules to retain molecules water and induced a loosened structure, amounting to a bigger mean pore size. This theory is supported by the characteristic results in section 3.2.

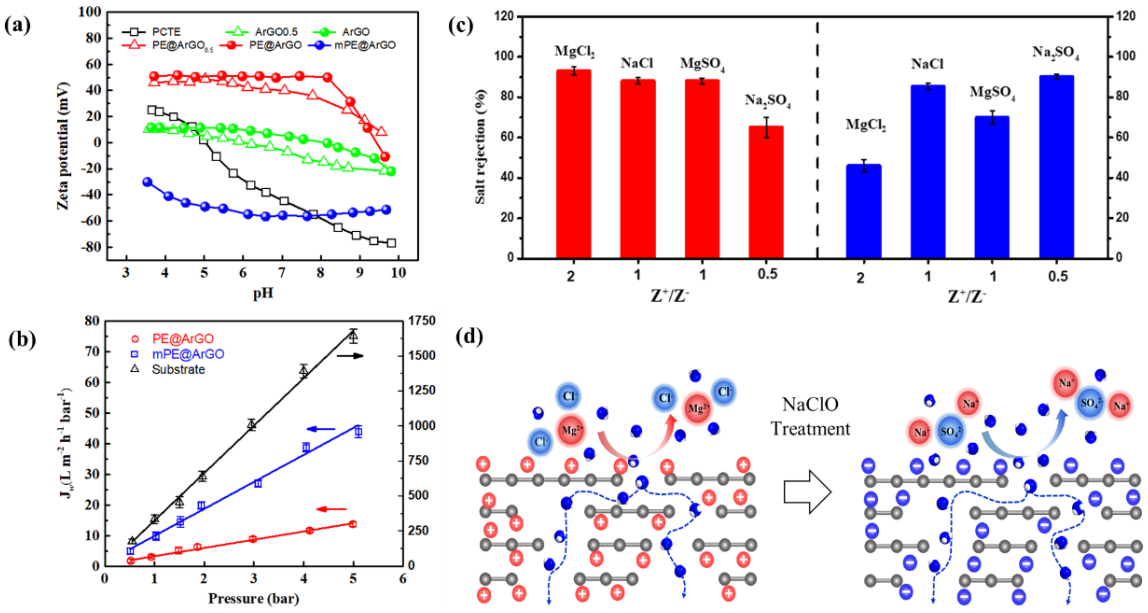


**Figure 7.** (a) The surface zeta potential of PCTE, ArGO, PE@ArGO and mPE@ArGO membranes; (b) The $J_w$–$\Delta P$ plot of PCTE substrate (black), mPE@ArGO (blue), and PE@ArGO membrane (red); (c) The rejections of PE@ArGO (red) and mPE@ArGO (blue) membranes for salts with different $Z^+/Z^-$ values; (d) An illustration depicting the preferential rejection to high valent co-ions by PE@ArGO and mPE@ArGO membranes;

3.5 Salt rejection test performance for PE@ArGO and mPE@ArGO membranes. In general, salt rejection of a membrane is governed by the combined effects of charge repulsion and size exclusion. Four model salts, $MgCl_2$, $MgSO_4$, NaCl, and $Na_2SO_4$, with varied $Z^+$ (charge number for the cation), $Z^-$ (charge number for the anion) and $Z^+/Z^-$ values, are selected to study the impact of the membrane charges on the solute rejection. The salt rejection of the positively charged PE@ArGO membrane decreased for salts with smaller $Z^+/Z^-$ values (93.0% for $MgCl_2$ > 88.1 to 88.2% for NaCl and $MgSO_4$ > 65.1% for $Na_2SO_4$, see Figure 7c). In contrast, the salt rejection of the negatively charged mPE@ArGO membrane follows an opposite trend, i.e., greater salt rejection for smaller $Z^+/Z^-$ values (42.9% for $MgCl_2$ < 68.3% for $MgSO_4$ < 85.4% for NaCl < 90.3%

for $Na_2SO_4$). These results agree well with the Donnan exclusion theory [36]. The lower rejection of $MgSO_4$ compared to that of NaCl (both with a $Z^+/Z^-$ value of 1) of the mPE@ArGO membrane can be explained by the greater charge screening effect by the divalent ions, which results in a weakened charge repulsion. However, the rejection values of $MgSO_4$ and NaCl were nearly identical for the PE@ArGO membrane. PE@ArGO had smaller channel size such that the size exclusion mechanism could play a more important role; this effect would favor the rejection of $MgSO_4$ compared to NaCl (hydrated radius of $Mg^{2+}$ (0.428 nm) > $Na^+$ (0.358 nm) and that of $SO_4^{2-}$ (0.379 nm) > $Cl^-$ (0.332 nm)). Therefore, the greater size exclusion effect of $MgSO_4$ compensates for its weaker charge repulsion in the case of the PE@ArGO membrane with tighter channels, leading to similar rejections to $MgSO_4$ and NaCl. The greater size exclusion effect for the PE@ArGO membrane is also reflected by its greater rejection values compared to the mPE@ArGO membrane for salts of $Z^+/Z^- = 1$ (symmetrical salts), and it is more obvious for $MgSO_4$ (with weakened charge repulsion effect compared to NaCl such that size exclusion plays a more dominant role).

The PE@ArGO membranes have superior NaCl rejection over the reported GOBMs prior to this work. Its separation performance is very competitive even compared with commercial NF membranes (Table 4). Such high performance is attributable to: 1) the engineered high charge density at PE@ArGO membrane surface which gates the transport of high valent co-ions; 2) the confined space between PE@ArGO nanosheets which acts as nanochannels; 3) The high charge density of PE@ArGO, bridging effect of PE molecules, and the in-situ assembly of PAH@ArGO and PSS@ArGO ensure the formation of a compact layered structure, avoiding the formation of wrinkles and bubbles which further lead to microstructural defects. Interestingly, when treated with NaOCl, the mPE@ArGO membrane can maintain the rejection at almost the same level while

the water permeability triples. In fact, the mPE@ArGO exhibits higher flux than most of the reported GOBMs while showing high rejection towards NaCl (85.4%), this value is better than the commercial NF membranes (Figure 8). It is of great value to further engineer the charge density and interspace of nanochannels to refine the design of the future generations of GOBMs.

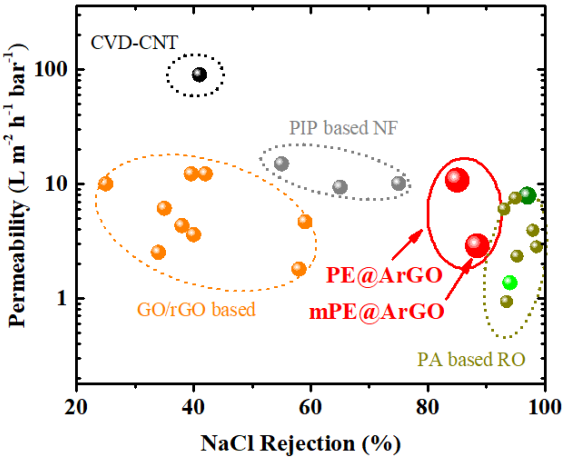


**Figure 8.** NaCl rejection and water permeability comparison between PE@ArGO membranes, literature reported GOBMs, and commercial polyamide based membranes.[9, 13-15, 62-69]

3.6 Dye rejection test performance for PE@ArGO membrane. To investigate the charge effect on slightly larger molecules, we explored the nanofiltration test of a series of dye molecules with varied molecular weight (300-1400 Da) using PE@ArGO and mPE@ArGO membranes. Interestingly, the positively charged PE@ArGO membranes had good rejection (>99.5 %) for all 5 dyes, regardless of the charge property (Table 5). The filtrates of dye solutions are nearly colorless (Figure 9). Conventionally, negatively charged GO based membranes are found to have low rejections to positively charged dyes, such as RhB.[9, 15, 26] However, positively charged dyes, such as RhB and MB, are highly rejected by the PE@ArGO and mPE@ArGO membranes. We attribute this good sieving ability to the bridging effect of highly charged PAH molecules between ArGO nanosheets, which not only reduces the intrinsic defects at loosely stacked regions but also

forms a dense self-assembled nanofilm with the PSS@GO intermediate layer that fills the gap between ArGO nanosheets. Size exclusion mechanism plays a dominant role here as indicated by the good rejection obtained by the molecules with size ranging from 1.4 nm to 4.4 nm (According to the estimation by an MM2 method using Chem3D[9]) regardless of cationic or anionic dyes. Nonetheless, charge exclusion still plays a minor role here as the positively charged MB is slightly better rejected than the negatively charged bigger molecules such as CR, RB5, and DR80. It is worth to note that the molecular sizes for the dyes serve only as an indication here as their charge, functional groups, and molecular shape are non-uniform. Thus these results could not represent the actual molecule weight cut-off (MWCO) of the PE@ArGO membranes.

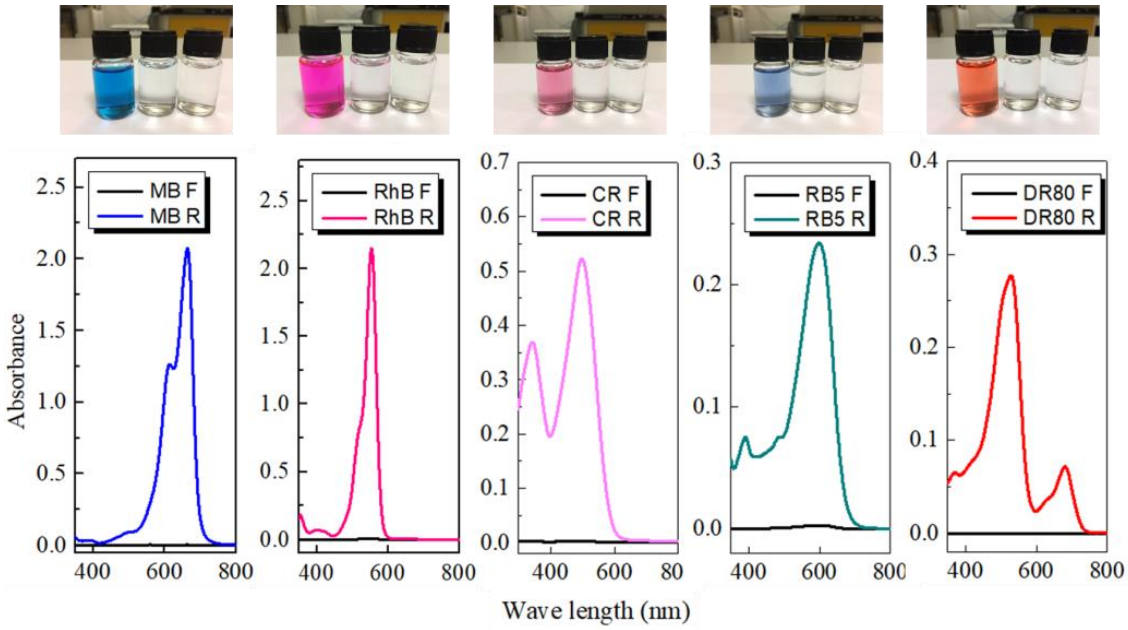


**Figure 9.** The optical image (upper) and UV-Vis adsorption spectrum (below) comparison between feed and filtrate solutions for MB, RhB, CR, RB5, and DR80. The rightmost vial in the optical images contains DI water reference.

For the negatively charged mPE@ArGO membranes, the rejection of all dyes is significantly lower than PE@ArGO membrane. Among them, positively charged and smaller dye molecules

have a larger pass rate (MB and RhB); while negatively charged and bigger dye molecules are better rejected. These tests are consistent with the salt rejection results where the increased pore diameter of the mPE@ArGO membrane deteriorates the rejection. The most significant decrease happens to the MB molecules, where the rejection dropped significantly to 95.2 %. Hence, it could be inferred that the rejection for even smaller molecules will decrease further. The actual pore size of the PE@ArGO/mPE@ArGO membranes should be less than the size of MB molecule (1.4 nm).

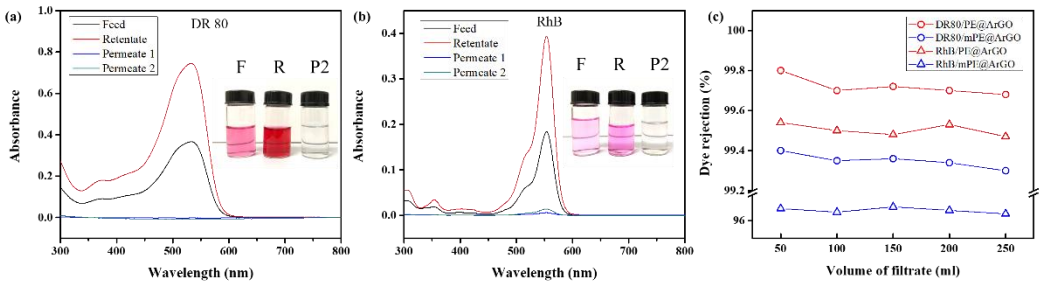


**Figure 10.** (a) The UV-Vis spectrum of DR 80 feed solution (10 ppm), the retentate (concentrate collected from the cell), permeate collected at 50 ml filtrate (Permeate 1), and the permeate collected at 250 ml filtrate (Permeate 2); and (b) The UV-Vis spectrum of RhB feed solution, retentate, permeate 1, and permeate 2 after the filtration by the mPE@ArGO membrane. (c) The dye rejections versus volume of filtrate for PE@ArGO and mPE@ArGO membranes;

Finally, continuous DR 80 (anionic) and RhB (cationic) filtration experiments were carried out to investigate the dye rejection stability. Both dye solutions were concentrated by approximately 2 times (Figure 10a and 10b) as 250 ml of filtrate was collected. Meanwhile, the rejection of membrane was maintained at the same level. This suggest the dye molecules have been mainly rejected and accumulated in the retentate rather than absorbed on the mPE@ArGO membrane surface.

## 4. Conclusion

We have developed novel PE@ArGO/mPE@ArGO membranes with tunable intercalated charges, continuously ordered and multi-layered structure, and long-term stability in water. Compared with conventional GOBMs and even some commercial polyamide based NF membranes, the PE@ArGO membranes have much smoother separation layers and more competitive separation performance (Figure 8). The Donnan charge exclusion mechanism induced by high surface $\delta_s$ was found to dominate the rejection of salts. Apart from salt ions, very high rejection to both cationic and anionic dye molecules with size ranging from 1.4 nm to 4.4 nm are observed for both membranes. We infer that the PE@ArGO/mPE@ArGO membranes should have a mean pore size less than the molecular size of MB (1.4 nm). In fact, the achievement of high rejection for both cationic and anionic dye molecules had rarely been reported for GOBMs. This can be explained by the elimination of micro-defects in layered PE@ArGO membranes by the bridging effect of PAH molecules and the in-situ self-assembly of PAH@ArGO/PSS@GO nanosheets.

With the possibility to engineer the charge density and interspace of nanochannels, the PE@ArGO membrane opens valuable opportunities to new designs of future generations of GOBMs with better charge and mass selectivity. Further study needs to understand the pore size, free volume and charge density distribution to optimize the charge gating ion exclusion effect. For example, more studies on membrane pore size are to be carried out using neutral solutes to isolate the size exclusion mechanism out of Donnan exclusion. Further, by engineering the charge and pore size properties of the nanochannels, we can expect to accurately sieve molecules that differ in mass and charge. For considerations in realistic production, the novel PE@ArGO material can

be applied using versatile approaches such as, dip coating, vacuum filtration, LbL assembly, and slot casting etc.

**Table 1. C1s, N1s, O1s atomic ratio for GO, PSS@GO, ArGO, PAH@ArGO nanosheets and PE@ArGO, mPE@ArGO membranes.**

| Sample | C1s (At. %) | N1s (At. %) | O1s (At. %) |
|---|---|---|---|
| GO NS | 68.0 | 0.7 | 31.4 |
| PSS@GO | 69.2 | 0.5 | 29.0 |
| ArGO NS | 88.4 | 5.4 | 6.2 |
| PAH@ArGO | 81.1 | 10.9 | 8.0 |
| PE@ArGO | 92.5 | 4.9 | 2.4 |
| mPE@ArGO | 89.9 | 4.9 | 4.9 |

**Table 2. The pure water permeability and surface properties for PE@ArGO and mPE@ArGO membranes.**

| Membrane | PWP ($L\ m^{-2}\ h^{-1}\ bar^{-1}$) | WCA (degree) | RMS (nm) | SAD (%) | $-\Delta G_{SL}$ ($mJ\ m^{-2}$) | $\delta_s$ ($mC/m^2$) |
|---|---|---|---|---|---|---|
| PE@ArGO | 2.9±0.5 | 42.3±2.0 | 19.2 | 25.26% | 116.8 | +4.37 |
| mPE@ArGO | 10.8±1.2 | 35.8±1.4 | 24.3 | 33.09% | 117.2 | -4.28 |

**Table 3. The FTIR absorption peaks assignment for PE@ArGO and mPE@ArGO membranes.**

| NO. | Wavenumber ($cm^{-1}$) | Assignment |
|---|---|---|
| 1 | ~1750 | C=O Stretching |
| 2 | 1520, 1625 | N-H Bending |
| 3 | ~2850-2950 | C-H Stretching |
| 4 | ~3300-3600 | N-H Stretching |
| 5 | 3300 | O-H Stretching |

**Table 4. The comparison of NaCl rejection with other GOBMs and commercial membranes**

| **Membrane** | **Preparation method** | **Feed concentration (NaCl)** | **Applied pressure (bar)** | **Water permeability ($L\ m^{-2}\ h^{-1}\ bar^{-1}$)** | **Rejection (%)** | **Ref.** |
|---|---|---|---|---|---|---|
| PE@ArGO | PE-VF | 1mM | 5 | 2.9±0.5 | 88.2±1.5 | This work |
| mPE@ArGO | PE-VF | 1mM | 5 | 10.8±1.2 | 85.4±1.8 | This work |
| GO/PEI | LbL | 1000ppm | 5 | 4.3 | 38 | [62] |
| GO/PEI | LbL | 500ppm | 1 | 6.1 | 42 | [63] |
| GO/HPEI/EDA | LbL | 1000ppm | 3 | 1.8 | 58 | [64] |
| GO/Porphyrin | VF | 2000ppm | 8 | 10.1 | 25 | [13] |
| RGO/CNT | VF | 10mM | 5 | 4.7 | 59 | [15] |
| RGO | VF | 20mM | 5 | 3.6 | 40 | [9] |
| RGO/CNT | VF | 10mM | 5 | 12.2 | 39.6 | [14] |
| PA-NF (NF270) | TFC | 10mM | 14 | 15.1 | 55 | [65] |
| PA-RO (BW30) | TFC | 10mM | 14 | 3.9 | 97.9 | [66] |

**Table 5. The dye rejection rates for PE@ArGO and mPE@ArGO membranes.**

| Dye | Charge | Molecular Weight (Da) | Molecular Size[a] (Angstrom) | Rejection (%) | |
|---|---|---|---|---|---|
| | | | | PE@ArGO | mPE@ArGO |
| MB | Positive | 320 | 14 | 99.8±0.2 | 95.2±0.5 |
| RhB | Positive | 479 | 15 | 99.5±0.1 | 96.7±0.7 |
| CR | Negative | 697 | 25 | 99.5±0.15 | 98.2±0.2 |
| RB5 | Negative | 992 | 20 | 99.6±0.12 | 99.1±0.15 |
| DR80 | Negative | 1373 | 44 | 99.7±0.1 | 99.3±0.1 |

Note: a. The molecular size is estimated by calculating the molecular length using a Molecular Mechanics 2 method in Chem3D software.

ASSOCIATED CONTENT

**Supporting Information**.

The following files are available free of charge.

Synthesis of GO, Fabrication of ArGO membrane, FESEM image of PCTE substrate, $ArGO_{0.5}$, $PE@ArGO_{0.5}$, and the cross-section of ArGO membranes. (PDF)

AUTHOR INFORMATION

**Corresponding Author**

*Chuyang. Y. Tang. Email: tangc@hku.edu

*James A. Prince. Email: jap2@np.edu.sg

**Funding Sources**

National Key Technologies R&D Program of China (No. 2017YFC0403903),

National Natural Science Foundation of China (No. 21706231)

Research & Innovation Scheme (IRIS) administered by Public Utility Board (PUB) of Singapore (No. 1501-IRIS-05).

ACKNOWLEDGMENT

Financial support from National Key Technologies R&D Program of China (No. 2017YFC0403903), National Natural Science Foundation of China (No. 21706231), and the Research & Innovation Scheme (IRIS) administered by Public Utility Board (PUB), Singapore (No. 1501-IRIS-05) are kindly acknowledged.

REFERENCES

1. Elimelech, M.; Phillip, W. A., The Future of Seawater Desalination: Energy, Technology, and the Environment. *Science* **2011,** *333*, 712-717.
2. Werber, J. R.; Osuji, C. O.; Elimelech, M., Materials for next-generation desalination and water purification membranes. *Nature Reviews Materials* **2016,** *1*, 16018.
3. Cadotte, J. E.; Petersen, R. J.; Larson, R. E.; Erickson, E. E., A new thin-film composite seawater reverse osmosis membrane. *Desalination* **1980,** *32*, 25-31.
4. Song, X.; Qi, S.; Tang, C. Y.; Gao, C., Ultra-thin, multi-layered polyamide membranes: Synthesis and characterization. *Journal of Membrane Science* **2017,** *540*, 10-18.
5. Zheng, Z.; Grünker, R.; Feng, X., Synthetic Two‐Dimensional Materials: A New Paradigm of Membranes for Ultimate Separation. *Advanced Materials* **2016,** *28*, 6529-6545.
6. Mi, B., Graphene Oxide Membranes for Ionic and Molecular Sieving. *Science* **2014,** *343*, 740-742.
7. Chen, B.; Jiang, H.; Liu, X.; Hu, X., Molecular Insight into Water Desalination across Multilayer Graphene Oxide Membranes. *ACS Applied Materials & Interfaces* **2017,** *9*, 22826-22836.
8. Pei, J. X.; Zhang, X. T.; Huang, L.; Jiang, H. F.; Hu, X. J., Fabrication of reduced graphene oxide membranes for highly efficient water desalination. *Rsc Advances* **2016,** *6*, 101948-101952.
9. Han, Y.; Xu, Z.; Gao, C., Ultrathin Graphene Nanofiltration Membrane for Water Purification. *Advanced Functional Materials* **2013,** *23*, 3693-3700.
10. Zhu, Y.; Murali, S.; Cai, W.; Li, X.; Suk, J. W.; Potts, J. R.; Ruoff, R. S., Graphene and Graphene Oxide: Synthesis, Properties, and Applications. *Advanced Materials* **2010,** *22*, 3906-3924.

11. Nair, R. R.; Wu, H. A.; Jayaram, P. N.; Grigorieva, I. V.; Geim, A. K., Unimpeded Permeation of Water Through Helium-Leak–Tight Graphene-Based Membranes. *Science* **2012,** *335*, 442-444.
12. Hung, W.-S.; Tsou, C.-H.; De Guzman, M.; An, Q.-F.; Liu, Y.-L.; Zhang, Y.-M.; Hu, C.-C.; Lee, K.-R.; Lai, J.-Y., Cross-Linking with Diamine Monomers To Prepare Composite Graphene Oxide-Framework Membranes with Varying d-Spacing. *Chemistry of Materials* **2014,** *26*, 2983-2990.
13. Xu, X.-L.; Lin, F.-W.; Du, Y.; Zhang, X.; Wu, J.; Xu, Z.-K., Graphene Oxide Nanofiltration Membranes Stabilized by Cationic Porphyrin for High Salt Rejection. *ACS Applied Materials & Interfaces* **2016,** *8*, 12588-12593.
14. Sun, P.; Chen, Q.; Li, X.; Liu, H.; Wang, K.; Zhong, M.; Wei, J.; Wu, D.; Ma, R.; Sasaki, T.; Zhu, H., Highly efficient quasi-static water desalination using monolayer graphene oxide/titania hybrid laminates. *NPG Asia Mater* **2015,** *7*, e162.
15. Gao, S. J.; Qin, H.; Liu, P.; Jin, J., SWCNT-intercalated GO ultrathin films for ultrafast separation of molecules. *Journal of Materials Chemistry A* **2015,** *3*, 6649-6654.
16. Nam, Y. T.; Choi, J.; Kang, K. M.; Kim, D. W.; Jung, H.-T., Enhanced Stability of Laminated Graphene Oxide Membranes for Nanofiltration via Interstitial Amide Bonding. *ACS Applied Materials & Interfaces* **2016,** *8*, 27376-27382.
17. Hu, M.; Mi, B., Enabling Graphene Oxide Nanosheets as Water Separation Membranes. *Environmental Science & Technology* **2013,** *47*, 3715-3723.
18. Werber, J. R.; Deshmukh, A.; Elimelech, M., The Critical Need for Increased Selectivity, Not Increased Water Permeability, for Desalination Membranes. *Environmental Science and Technology Letters* **2016,** *3*, 112-120.
19. Weng, X. D.; Bao, X. J.; Jiang, H. D.; Chen, L.; Ji, Y. L.; An, Q. F.; Gao, C. J., pH-responsive nanofiltration membranes containing carboxybetaine with tunable ion selectivity for charge-based separations. *Journal of Membrane Science* **2016,** *520*, 294-302.
20. Lin, Z.; Zhang, Q.; Qu, Y.; Chen, M.; Soyekwo, F.; Lin, C.; Zhu, A.; Liu, Q., LBL assembled polyelectrolyte nanofiltration membranes with tunable surface charges and high permeation by employing a nanosheet sacrificial layer. *Journal of Materials Chemistry A* **2017,** *5*, 14819-14827.
21. Zhang, C.; Wei, K.; Zhang, W.; Bai, Y.; Sun, Y.; Gu, J., Graphene Oxide Quantum Dots Incorporated into a Thin Film Nanocomposite Membrane with High Flux and Antifouling Properties for Low-Pressure Nanofiltration. *ACS Applied Materials and Interfaces* **2017,** *9*, 11082-11094.
22. Li, D.; Muller, M. B.; Gilje, S.; Kaner, R. B.; Wallace, G. G., Processable aqueous dispersions of graphene nanosheets. *Nat Nano* **2008,** *3*, 101-105.
23. Sun, P.; Wang, K.; Zhu, H., Recent Developments in Graphene‐Based Membranes: Structure, Mass‐Transport Mechanism and Potential Applications. *Advanced Materials* **2016,** *28*, 2287-2310.
24. Oh, Y.; Armstrong, D. L.; Finnerty, C.; Zheng, S.; Hu, M.; Torrents, A.; Mi, B., Understanding the pH-responsive behavior of graphene oxide membrane in removing ions and organic micropollulants. *Journal of Membrane Science* **2017,** *541*, 235-243.
25. Abraham, J.; Vasu, K. S.; Williams, C. D.; Gopinadhan, K.; Su, Y.; Cherian, C. T.; Dix, J.; Prestat, E.; Haigh, S. J.; Grigorieva, I. V.; Carbone, P.; Geim, A. K.; Nair, R. R., Tunable sieving of ions using graphene oxide membranes. **2017,** *12*, 546.

26. Morelos-Gomez, A.; Cruz-Silva, R.; Muramatsu, H.; Ortiz-Medina, J.; Araki, T.; Fukuyo, T.; Tejima, S.; Takeuchi, K.; Hayashi, T.; Terrones, M.; Endo, M., Effective NaCl and dye rejection of hybrid graphene oxide/graphene layered membranes. *Nat Nano* **2017**, DOI: 10.1038/nnano.2017.1160.
27. Chen, L.; Shi, G.; Shen, J.; Peng, B.; Zhang, B.; Wang, Y.; Bian, F.; Wang, J.; Li, D.; Qian, Z.; Xu, G.; Liu, G.; Zeng, J.; Zhang, L.; Yang, Y.; Zhou, G.; Wu, M.; Jin, W.; Li, J.; Fang, H., Ion sieving in graphene oxide membranes via cationic control of interlayer spacing. *Nature* **2017,** *DOI: 10.1038/nature24044*.
28. Zambare, R.; Song, X.; Bhuvana, S.; Antony Prince, J. S.; Nemade, P., Ultrafast Dye Removal Using Ionic Liquid–Graphene Oxide Sponge. *ACS Sustainable Chemistry & Engineering* **2017,** *5*, 6026-6035.
29. Chen, J.; Hamon, M. A.; Hu, H.; Chen, Y.; Rao, A. M.; Eklund, P. C.; Haddon, R. C., Solution Properties of Single-Walled Carbon Nanotubes. *Science* **1998,** *282*, 95-98.
30. Saren, Q.; Qiu, C. Q.; Tang, C. Y., Synthesis and Characterization of Novel Forward Osmosis Membranes based on Layer-by-Layer Assembly. *Environmental Science & Technology* **2011,** *45*, 5201-5208.
31. Ariza, M. J.; Benavente, J., Streaming potential along the surface of polysulfone membranes: a comparative study between two different experimental systems and determination of electrokinetic and adsorption parameters. *Journal of Membrane Science* **2001,** *190*, 119-132.
32. Song, X.; Liu, Z.; Sun, D. D., Nano Gives the Answer: Breaking the Bottleneck of Internal Concentration Polarization with a Nanofiber Composite Forward Osmosis Membrane for a High Water Production Rate. *Advanced Materials* **2011,** *23*, 3256-3260.
33. Zambare, R. S.; Dhopte, K. B.; Patwardhan, A. V.; Nemade, P. R., Polyamine functionalized graphene oxide polysulfone mixed matrix membranes with improved hydrophilicity and anti-fouling properties. *Desalination* **2017,** *403*, 24.
34. Zhao, F.-Y.; Ji, Y.-L.; Weng, X.-D.; Mi, Y.-F.; Ye, C.-C.; An, Q.-F.; Gao, C.-J., High-Flux Positively Charged Nanocomposite Nanofiltration Membranes Filled with Poly(dopamine) Modified Multiwall Carbon Nanotubes. *ACS Applied Materials & Interfaces* **2016,** *8*, 6693-6700.
35. Ghosh, A. K.; Jeong, B.-H.; Huang, X.; Hoek, E. M. V., Impacts of reaction and curing conditions on polyamide composite reverse osmosis membrane properties. *Journal of Membrane Science* **2008,** *311*, 34-45.
36. Schaep, J.; Van der Bruggen, B.; Vandecasteele, C.; Wilms, D., Influence of ion size and charge in nanofiltration. *Separation and Purification Technology* **1998,** *14*, 155-162.
37. Yang, H.; Shan, C.; Li, F.; Han, D.; Zhang, Q.; Niu, L., Covalent functionalization of polydisperse chemically-converted graphene sheets with amine-terminated ionic liquid. *Chemical Communications* **2009**, 3880-3882.
38. Childress, A. E.; Elimelech, M., Relating Nanofiltration Membrane Performance to Membrane Charge (Electrokinetic) Characteristics. *Environmental Science & Technology* **2000,** *34*, 3710-3716.
39. Blagbrough, I. S.; Metwally, A. A.; Geall, A. J., Measurement of Polyamine pK a Values. In *Polyamines: Methods and Protocols*, Pegg, A. E.; Casero, J. R. A., Eds. Humana Press: Totowa, NJ, **2011**, pp 493-503.
40. Qiu, C.; Qi, S.; Tang, C. Y., Synthesis of high flux forward osmosis membranes by chemically crosslinked layer-by-layer polyelectrolytes. *Journal of Membrane Science* **2011,** *381*, 74-80.

41. Kovtyukhova, N. I.; Ollivier, P. J.; Martin, B. R.; Mallouk, T. E.; Chizhik, S. A.; Buzaneva, E. V.; Gorchinskiy, A. D., Layer-by-Layer Assembly of Ultrathin Composite Films from Micron-Sized Graphite Oxide Sheets and Polycations. *Chemistry of Materials* **1999,** *11*, 771-778.
42. Choi, W.; Choi, J.; Bang, J.; Lee, J.-H., Layer-by-Layer Assembly of Graphene Oxide Nanosheets on Polyamide Membranes for Durable Reverse-Osmosis Applications. *ACS Applied Materials & Interfaces* **2013,** *5*, 12510-12519.
43. Hong, T.-K.; Lee, D. W.; Choi, H. J.; Shin, H. S.; Kim, B.-S., Transparent, Flexible Conducting Hybrid Multilayer Thin Films of Multiwalled Carbon Nanotubes with Graphene Nanosheets. *ACS Nano* **2010,** *4*, 3861-3868.
44. Chong, J. Y.; Aba, N. F. D.; Wang, B.; Mattevi, C.; Li, K., UV-Enhanced Sacrificial Layer Stabilised Graphene Oxide Hollow Fibre Membranes for Nanofiltration. *Scientific Reports* **2015,** *5*, 15799.
45. Kulkarni, D. D.; Choi, I.; Singamaneni, S. S.; Tsukruk, V. V., Graphene Oxide−Polyelectrolyte Nanomembranes. *ACS Nano* **2010,** *4*, 4667-4676.
46. Park, S.; Dikin, D.; Nguyen, S.; Ruoff, R., Graphene Oxide Sheets Chemically Cross-Linked by Polyallylamine. *The journal of physical chemistry. C* **2009,** *113*, 15801-15804.
47. Shen, J.; Liu, G.; Huang, K.; Chu, Z.; Jin, W.; Xu, N., Subnanometer Two-Dimensional Graphene Oxide Channels for Ultrafast Gas Sieving. *ACS Nano* **2016,** *10*, 3398-3409.
48. Boussu, K.; Van der Bruggen, B.; Volodin, A.; Snauwaert, J.; Van Haesendonck, C.; Vandecasteele, C., Roughness and hydrophobicity studies of nanofiltration membranes using different modes of AFM. *Journal of Colloid and Interface Science* **2005,** *286*, 632-638.
49. Boussu, K.; Van der Bruggen, B.; Volodin, A.; Van Haesendonck, C.; Delcour, J. A.; Van der Meeren, P.; Vandecasteele, C., Characterization of commercial nanofiltration membranes and comparison with self-made polyethersulfone membranes. *Desalination* **2006,** *191*, 245-253.
50. Do, V. T.; Tang, C. Y.; Reinhard, M.; Leckie, J. O., Effects of Chlorine Exposure Conditions on Physiochemical Properties and Performance of a Polyamide Membrane—Mechanisms and Implications. *Environmental Science & Technology* **2012,** *46*, 13184-13192.
51. Kang, G.-D.; Gao, C.-J.; Chen, W.-D.; Jie, X.-M.; Cao, Y.-M.; Yuan, Q., Study on hypochlorite degradation of aromatic polyamide reverse osmosis membrane. *Journal of Membrane Science* **2007,** *300*, 165-171.
52. Kwon, Y.-N.; Leckie, J. O., Hypochlorite degradation of crosslinked polyamide membranes: II. Changes in hydrogen bonding behavior and performance. *Journal of Membrane Science* **2006,** *282*, 456-464.
53. Soice, N. P.; Maladono, A. C.; Takigawa, D. Y.; Norman, A. D.; Krantz, W. B.; Greenberg, A. R., Oxidative degradation of polyamide reverse osmosis membranes: Studies of molecular model compounds and selected membranes. *Journal of Applied Polymer Science* **2003,** *90*, 1173-1184.
54. Simon, A.; Nghiem, L. D.; Le-Clech, P.; Khan, S. J.; Drewes, J. E., Effects of membrane degradation on the removal of pharmaceutically active compounds (PhACs) by NF/RO filtration processes. *Journal of Membrane Science* **2009,** *340*, 16-25.
55. Kim, K. J.; Fane, A. G.; Nystrom, M.; Pihlajamaki, A.; Bowen, W. R.; Mukhtar, H., Evaluation of electroosmosis and streaming potential for measurement of electric charges of polymeric membranes. *Journal of Membrane Science* **1996,** *116*, 149-159.

56. Moya, S.; Dähne, L.; Voigt, A.; Leporatti, S.; Donath, E.; Möhwald, H., Polyelectrolyte multilayer capsules templated on biological cells: core oxidation influences layer chemistry. *Colloids and Surfaces A: Physicochemical and Engineering Aspects* **2001,** *183-185*, 27-40.
57. Gregurec, D.; Olszyna, M.; Politakos, N.; Yate, L.; Dahne, L.; Moya, S. E., Stability of polyelectrolyte multilayers in oxidizing media: a critical issue for the development of multilayer based membranes for nanofiltration. *Colloid and Polymer Science* **2015,** *293*, 381-388.
58. Yip, N. Y.; Elimelech, M., Performance Limiting Effects in Power Generation from Salinity Gradients by Pressure Retarded Osmosis. *Environmental Science & Technology* **2011,** *45*, 10273-10282.
59. Kharlampieva, E.; Kozlovskaya, V.; Sukhishvili, S. A., Layer-by-Layer Hydrogen-Bonded Polymer Films: From Fundamentals to Applications. *Advanced Materials* **2009,** *21*, 3053-3065.
60. Zhang, Y.; Li, F.; Valenzuela, L. D.; Sammalkorpi, M.; Lutkenhaus, J. L., Effect of Water on the Thermal Transition Observed in Poly(allylamine hydrochloride)–Poly(acrylic acid) Complexes. *Macromolecules* **2016,** *49*, 7563-7570.
61. Do, V. T.; Tang, C. Y.; Reinhard, M.; Leckie, J. O., Degradation of Polyamide Nanofiltration and Reverse Osmosis Membranes by Hypochlorite. *Environmental Science & Technology* **2012,** *46*, 852-859.
62. Nan, Q.; Li, P.; Cao, B., Fabrication of positively charged nanofiltration membrane via the layer-by-layer assembly of graphene oxide and polyethylenimine for desalination. *Applied Surface Science* **2016,** *387*, 521-528.
63. Goh, K.; Setiawan, L.; Wei, L.; Si, R.; Fane, A. G.; Wang, R.; Chen, Y., Graphene oxide as effective selective barriers on a hollow fiber membrane for water treatment process. *Journal of Membrane Science* **2015,** *474*, 244-253.
64. Zhang, Y.; Zhang, S.; Gao, J.; Chung, T.-S., Layer-by-layer construction of graphene oxide (GO) framework composite membranes for highly efficient heavy metal removal. *Journal of Membrane Science* **2016,** *515*, 230-237.
65. Tang, C. Y.; Kwon, Y.-N.; Leckie, J. O., Effect of membrane chemistry and coating layer on physiochemical properties of thin film composite polyamide RO and NF membranes. *Desalination* **2009,** *242*, 168-182.
66. Tang, C. Y.; Fu, Q. S.; Robertson, A. P.; Criddle, C. S.; Leckie, J. O., Use of reverse osmosis membranes to remove perfluorooctane sulfonate (PFOS) from semiconductor wastewater. *Environ Sci Technol* **2006,** *40*, 7343-7349.
67. Jeong, B.-H.; Hoek, E. M. V.; Yan, Y.; Subramani, A.; Huang, X.; Hurwitz, G.; Ghosh, A. K.; Jawor, A., Interfacial polymerization of thin film nanocomposites: A new concept for reverse osmosis membranes. *Journal of Membrane Science* **2007,** *294*, 1-7.
68. Li, X.; Chou, S.; Wang, R.; Shi, L.; Fang, W.; Chaitra, G.; Tang, C. Y.; Torres, J.; Hu, X.; Fane, A. G., Nature gives the best solution for desalination: Aquaporin-based hollow fiber composite membrane with superior performance. *Journal of Membrane Science* **2015,** *494*, 68-77.
69. Holt, J. K.; Park, H. G.; Wang, Y.; Stadermann, M.; Artyukhin, A. B.; Grigoropoulos, C. P.; Noy, A.; Bakajin, O., Fast Mass Transport Through Sub-2-Nanometer Carbon Nanotubes. *Science* **2006,** *312*, 1034-1037.

TOC graph. High charge density polyelectrolyte intercalated ArGO membrane with tunable positive/negative charge with preferential rejection to high valent cations/anions.